

SparseDC: Depth Completion from sparse and non-uniform inputs

Chen Long^{1*} Wenxiao Zhang^{2*} Zhe Chen¹ Haiping Wang¹
 Yuan Liu³ Zhen Cao¹ Zhen Dong^{1†} Bisheng Yang^{1†}

¹Wuhan University ²Singapore University of Technology and Design ³The University of Hong Kong
 {chenlong107, ChenZhe_WHU, hpwang, zhen.cao, dongzhenwhu, bshyang}@whu.edu.cn

wenxxiao.zhang@gmail.com, yuanly@connect.hku.hk

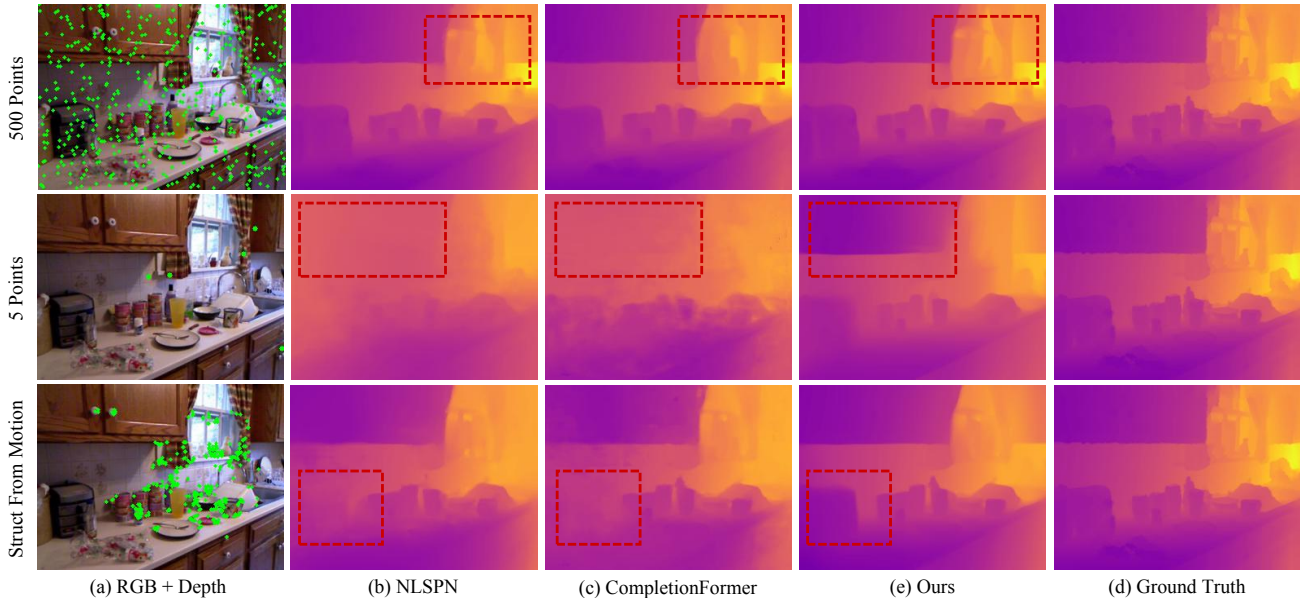


Figure 1. **Depth Completion from sparse and non-uniform inputs.** From top to bottom, we show the completed depth of state-of-the-art methods and ours using 500 depth points, 5 depth points, and non-uniform depth points obtained by SFM, respectively. Unlike the degradation of comparison methods, our framework can achieve reliable prediction under the above settings.

Abstract

We propose *SparseDC*, a model for *Depth Completion* of **Sparse** and non-uniform depth inputs. Unlike previous methods focusing on completing fixed distributions on benchmark datasets (e.g., NYU with 500 points, KITTI with 64 lines), *SparseDC* is specifically designed to handle depth maps with poor quality in real usage. The key contributions of *SparseDC* are two-fold. First, we design a simple strategy, called *SFFM*, to improve the robustness under sparse input by explicitly filling the unstable depth features with stable image features. Second, we propose a two-branch feature embedder to predict both the precise local geometry of regions with available depth values and accurate struc-

tures in regions with no depth. The key of the embedder is an uncertainty-based fusion module called *UFFM* to balance the local and long-term information extracted by CNNs and ViTs. Extensive indoor and outdoor experiments demonstrate the robustness of our framework when facing sparse and non-uniform input depths. The pre-trained model and code are available at <https://github.com/WHU-USI3DV/SparseDC>.

1. Introduction

Acquiring dense and accurate depth is crucial in various fields, such as autonomous driving[29, 55], 3D reconstruction[8, 26, 33], scene understanding[7, 21], AR/VR[35, 54]. Although the commonly used depth sensors, such as Microsoft Kinect[56], Intel RealSense[19],

*These authors contribute equally to this work.

†Corresponding authors.

LIDAR[2], can obtain depth within their effective field of view, it is still a great challenge to obtain dense depth maps due to environment, equipment, and cost limitations. In recent years, depth completion, serving as a cost-effective means to achieve dense pixel-wise depth, has become a long-standing research endeavor that has captivated the attention of many researchers.

Despite achieving impressive performance on benchmark datasets[9, 32], existing state-of-the-art methods[46, 51, 52, 58] often fall short in some challenging cases. In contrast to the fixed data distribution of the benchmark dataset(e.g., NYU Depth[32] with 500 points, Kitti[9] with 64 lines), the inputs in real scenarios may be non-uniform and sparser. For example, researchers often employ depth sensors with lower resolutions (Velodyne HDL-16E LiDAR, VCSEL ToF sensors) to mitigate costs. In addition, environmental factors easily influence sensors, such as high-reflectivity objects and multipath effects resulting in uneven distribution of effective depth points. Regrettably, mainstream methods primarily focus on the sparse-to-dense completion process without realizing the sparsity changes and the non-uniform distribution of depth points. Consequently, they are difficult to reconstruct the scene structure when the spatial pattern of the input significantly deviates from the distribution observed in the benchmark dataset during training, as illustrated in Fig. 1

The sparse and non-uniform input depth brings great challenges in extracting stable and robust features for the completion task. In the regions with dense input depth, the network needs to learn to trust the local dense input depth values while in regions with sparse or even no depth, the network is supposed to speculate the depth values from the RGB features and other long-term context information. However, the changing input depth patterns shown in Fig. 1(a) make the network confusing in which kind of features should be extracted even with data augmentation to simulate the changing depth in training [6, 10, 43, 47]. To solve this problem, we introduce *Sparse Feature Filling Module* that explicitly fills the unstable depth features with stable image features thereby improving the robustness of the network to various spatial distributions of input depth.

Furthermore, we observed that CNNs and ViTs show different characteristics in dealing with non-uniform input depths. In a simple experiment, we select ResNet-18[12] and PvtV2-b1[44, 45] as two backbone networks for the depth completion task and evaluate them on the NYU Depth V2[32] with input depth maps with varying densities. As illustrated in Fig. 2, though the overall performance of ResNet is better, as the density of input depth decreases, more and more depth values predicted by the PvtV2-b1 are more accurate than those predicted by the ResNet-18. The reason is that high-density depth points are sufficient to provide rich local context and detail for depth comple-

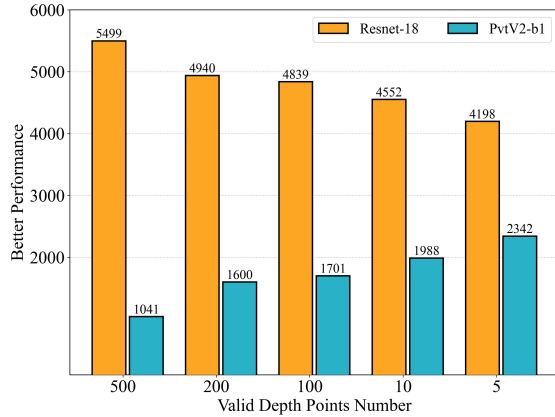


Figure 2. **Pilot study results on NYU Depth V2 dataset.** The horizontal axis represents the number of effective depth points in each testing depth map. The vertical axis illustrates the number of testing depth maps for which the network outperforms the other in terms of RMSE.

tion, while for low-density inputs, we need to understand the overall scene to fill large areas. Correspondingly, CNNs are known for their ability to extract local features with fine-grained details while ViTs focus on capturing the global scene context to leverage global relationships among pixels. The long-term context helps the ViT to account for the sparse input depth values. This observation motivates us to design a two-branch network structure that consists of both CNNs and ViTs to combine the advantages of both parts for a better depth completion on the sparse and non-uniform input depth maps.

An important problem here is how to fuse the two-branch features to get robust features. As discussed before, the network needs to put different importance on features from the CNNs and ViTs according to the local density of the input depth maps. However, a naive fusion [46, 52], which simply concatenate or add the features from two branches, actually treats features from two branches equally and thus leads to degenerated performances. To address this problem, we design an *Uncertainty-Guided Feature Fusion Module(UFFM)* to dynamically fuse extracted features explicitly. The UFFM uses sparse depths to estimate and correct the uncertainty of each pixel and utilizes this information to guide the fusion process, enabling the network to adjust the relative contribution of each branch based on the distribution patterns of the inputs.

In summary, we propose a novel deep completion framework named SparseDC, Fig. 3 illustrates the whole pipeline with above new components. SparseDC exhibits significant robustness improvement with better efficiency when dealing with sparse and non-uniform depths. We conduct a comprehensive experimental evaluation of our approach on

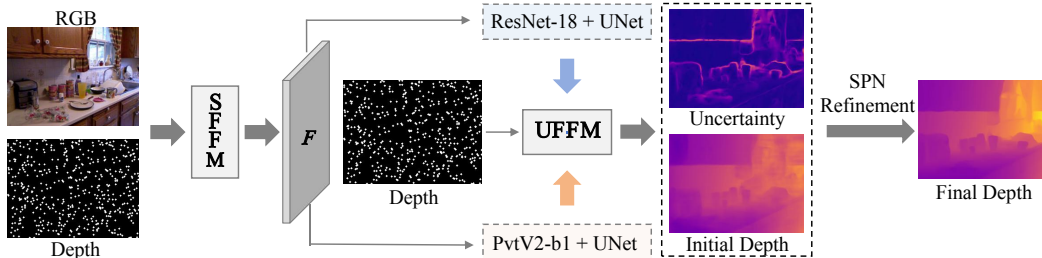


Figure 3. **SparseDC Architecture.** Given a sparse depth map and an image, we obtain a stable initial feature F using SFFM. Then, we adopt a two-branch feature extractor to get multi-scale features. After that, the extracted features and sparse depth map are fed to UFFM to obtain the initial depth and estimated uncertainty. Finally, a non-local propagation network[34] is exploited for final refinement.

NYU Depth[32], KITTI DC[9], and SUN RGB-D[41] and demonstrate 17% improvements on REL metric, 7.8% improvements on RMSE metric, respectively, over the State-of-the-art method CompletionFormer[52].

Overall, our contributions can be summarized as follows:

- We analyze the limitations of mainstream methods when dealing with sparse and non-uniform inputs and propose a novel depth completion framework called SparseDC to tackle this. It consists of several modules which can help extract stable and robust features for the completion task.
- We access the performance between ours and state-of-the-art methods on some simulated and real challenging cases using indoor[32, 41] and outdoor datasets[9]. Extensive experiments show the robustness of SparseDC when dealing with sparse and non-uniform depths.

2. Related Work

Depth Completion is a fundamental task in computer vision. It aims at recovering dense pixel-level depth from sparse depth maps obtained from sensors. In recent years, deep learning-based methods have emerged as the leading approaches to this task. Uhrig et al.[43] introduced sparse convolution as an alternative to traditional convolution and established benchmark datasets based on Kitti for evaluating depth completion algorithms. Later, Ma et al.[28] incorporated RGB data as an additional input, significantly improving the performance for the deep completion task. Building upon this[28], researchers have been growing interest in exploring multimodal data fusion in their frameworks, such as images[17, 24, 30, 36, 37, 57], normals[11, 50], semantics[31], and residual depth maps[23]. Then, Cheng et al. proposed a convolutional spatial propagation network CSPN[3], the first to apply spatial propagation techniques to depth completion. After that, methods such as CSPN++[4], NLSPN[34], DySPN[22], GraphCSPN[25], etc. have been proposed, they improve the accuracy and efficiency of depth completion by designing different convolution strategies (deformable convolution, graph convolution, etc.) to propagate the local information provided by the depth points over image, and achieve SOTA per-

formance on benchmark datasets. To push the envelope of depth completion, recent approaches tended to use complex network structures and sophisticated learning strategies[14, 46, 51, 58], such as BEV@DC[52], which proposed a more efficient and powerful multi-modal training scheme to boost the performance of image-guided depth completion. However, these methods mainly emphasize sparse-to-dense conversion without realizing the impact of sparsity changes and non-uniform depth points, which limits their scope of applications in real scenarios.

Some researchers have considered this problem and given their solutions. Andrea Conti et al. proposed SpAgNet[5]. The key idea is not to directly feed sparse depth points to the convolutional layers, but to iteratively merge the sparse input points with multiple depth maps predicted by the network during the decoding process. This approach mitigates the effects of uneven inputs. However, the receptive field of the depth points is very restricted, leading to the final result that relies on the performance of the backbone network, which increases the number of parameters of the model ($51M \gg 25.8M$ NLSPN[34]) and leads to a domain bias, limiting its applicability. Another related research is Sparse SPN[48], which propagates sparsely distributed depth values to the rest of the image by designing a cross-shaped spatial propagation network. However, this approach still relies on the local inductive bias provided by the spatial propagation technique, and has limited ability to model depth values over long ranges. In addition, Sparse SPN[48] is designed only for keypoint sampling, which cannot handle other spatial patterns such as uneven density and big holes.

3. Method

3.1. Overview

Given a sparse depth map $\mathcal{S} \in \mathbb{R}^{H \times W \times 1}$ and an image $\mathcal{I} \in \mathbb{R}^{H \times W \times 3}$, our goal is to restore a dense pixel-wise depth $\mathcal{D} \in \mathbb{R}^{H \times W \times 1}$. Different from mainstream methods, we focus on dealing with *sparse* and *non-uniform* inputs.

The whole pipeline of SparseDC is illustrated in Fig. 3.

First, we feed the depth map \mathcal{S} and image \mathcal{I} into the *SFFM* to obtain an initial feature map $\mathbf{F} \in \mathbb{R}^{H \times W \times C}$. Then, we embed \mathbf{F} with two separate feature extractors, composed by CNNs and ViTs, to respectively extract so-called local multi-scale features $\mathbf{F}_{local} = \{f_l^n\}_{n=0}^N$ and global multi-scale features $\mathbf{F}_{global} = \{f_g^n\}_{n=0}^N$, where f_*^n indicates the n^{th} scale feature map. After that, we design an *UFFM* to predict the pixel-wise uncertainty to guide the fusion of local features \mathbf{F}_{local} and global features \mathbf{F}_{global} at different scales. We thus get the fused features $\mathbf{F}_{fuse} = \{f_*^n\}_{n=0}^N$ to estimate the initial depth map and uncertainty. Finally, we apply the non-local spatial propagation module[34] to refine the initial depth map and get the final depth D .

3.2. Sparse Feature Fill Module

Given an image and a depth map, SFFM aims to output a feature map mitigating the feature instability[47] caused by non-uniform depths. As shown in Fig. 4, existing methods struggle to maintain the geometry shape in the face of non-uniform inputs, which can be alleviated by SFFM.

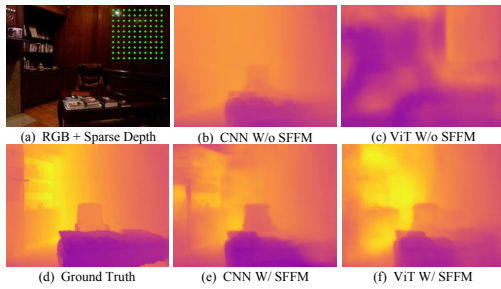


Figure 4. **Visual comparison.** Illustration of the effectiveness of our proposed SFFM on CNN and ViT backbones with non-uniform depth inputs.

Fig. 5 depicts the detailed structure of the SFFM. Given the sparse and non-uniform depth map \mathcal{S} and the image \mathcal{I} , we first extract the features of the image and depth with a stack of 2D convolution, batch normalization[16], and LeakyReLU[1, 49] layer. Then, we concatenate the image and depth features on the feature dimension. After that, we use gate convolution module[53] with channel attention to fuse these features. It learns the weights of the stable image features and sparse depth features based on the distribution of input depths, and use the weight to dynamically guide the feature filling to obtain \mathbf{F}'_{dep} . Finally, \mathbf{F}'_{dep} and \mathbf{F}_{rgb} are concatenated to obtain a stable feature input F by using another gated convolution layer. In addition, to control the feature range of F and accelerate the convergence of the model, we predict a coarse depth map D' by feeding F to an extra depth decoder head for intermediate supervision.

3.3. Two Branch Feature Extraction

Motivated by the observations in Fig. 2, we introduced a two-branch feature extraction architecture, one

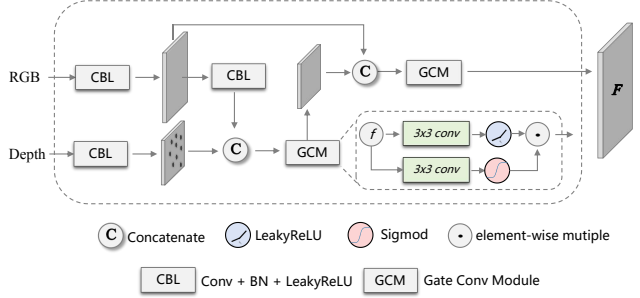


Figure 5. **An illustration of SFFM.** SFFM aims to output stable and robustness features for depth completion.

convolution-based branch focuses on extracting the local information provided by the depth points, called Local Branch, and the other branch is based on the vision transformer to provide indispensable global information, called Global Branch.

Local Branch. We choose ResNet-18[12] pretrained on ImageNet[20] as the backbone network of the convolution branch. Specifically, it downsamples the feature map \mathbf{F} to scales $\frac{1}{1}, \frac{1}{2}, \frac{1}{4}, \frac{1}{8}, \frac{1}{16}$. After that, the features will be used in the UNet[38] decoding step as input to get \mathbf{F}_{local} .

Global Branch. We chose the lightweight PvtV2-b1[45] also pre-trained on ImageNet[20] as our global feature extract backbone. This branch first splits the input Feature \mathbf{F} into 4×4 patches by a convolution filter with a kernel size of 7. After that, a linear embedding layer is applied to project the downsampled feature to an arbitrary dimension. Then, it uses 4 transformer layers to downsample the initial feature to $\frac{1}{1}, \frac{1}{4}, \frac{1}{8}, \frac{1}{16}, \frac{1}{32}$, and these features will also be used in decoding steps to get \mathbf{F}_{global} , like \mathbf{F}_{local} .

3.4. Uncertainty-Guide Feature Fusion Module

Given non-uniform and sparse inputs, the network needs to learn to trust the local dense input depth values in the regions with dense input depth. In regions with sparse or even no depth, the network is supposed to speculate the depth values from long-term context information.

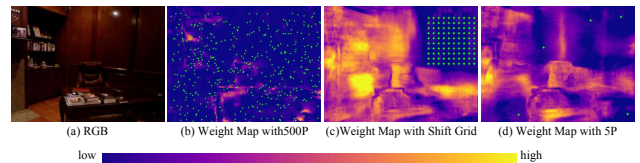


Figure 6. **Weight Map Visualization.** We visualize the weight map with different input patterns. The darker the color, the more the global branch contributes to the whole model.

To achieve this, we propose a weighted fusion strategy that enables the network to dynamically determine the confidence levels of local and global branch features. Specifically, we predict the pixel-wise uncertainty of each feature branch. Then, we use the input depth points to rectify the

uncertainty and finally use uncertainty to guide the explicit fusion of features. Fig. 6 illustrates the effect of UFFM in the face of sparse and non-uniform inputs. UFFM can adjust the contributions of each branch according to the inputs’ spatial pattern, realizing the complementary advantages of global and local information.

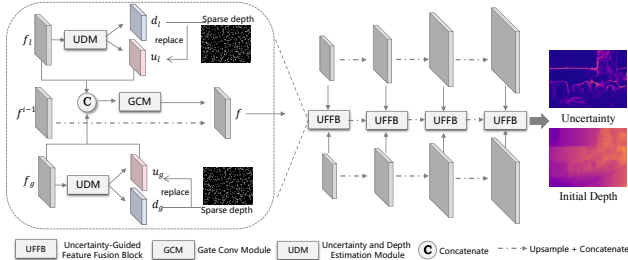


Figure 7. **UFFM Architecture.** UFFM aims to dynamically fuse the extracted features and then estimate the initial depth and reliable uncertainty.

In practice, UFFM applies several Uncertainty-guided Feature Fusion Block (UFFB) at different scales $\frac{1}{1}, \frac{1}{2}, \frac{1}{4}, \frac{1}{8}$. Fig. 7 illustrates the detailed structure of UFFM. Given the multi-scale local features \mathbf{F}_{local} and global features \mathbf{F}_{global} , UFFB first uses two different convolutional layers (depicted as UDM in Fig. 7) to compute an uncertainty and a depth map at this scale. These will be fed to the UFFB of the next scale to correct the predicted results iteratively. Since there is no ground truth for the uncertainty prediction, we compute a pseudo ground truth uncertainty inspired by [40], formulated in Eq. (1).

$$\hat{u} = 1 - \exp\left(-\frac{|d^n - g^n|}{b \times g^n}\right) \quad (1)$$

where, \hat{u} denotes the defined pseudo ground truth uncertainty, g^n is the ground truth depth map at scale n^{th} , the d^n is predicted depth maps. b is a coefficient that controls the tolerance for error, we set b as 0.1 in this paper to amplify differences between features. In addition, to further exploit the depth information, we downsample the sparse depth map \mathcal{S} by sparsity aware pooling to get multi-scale depth maps. After that, we use Eq. (1) to calculate the accurate uncertainty and replace the estimated uncertainty at positions that have valid depth points. Then, we use the predicted and replaced uncertainty to guide the fusion of different features as shown in Eq. (2).

$$f^n = Gate((1 - u_l^n) \cdot f_l^n \oplus (1 - u_g^n) \cdot f_g^n) \quad (2)$$

where, u_l^n denotes the local feature uncertainty, the u_g^n denotes the global feature uncertainty, and the f^n is the fused feature which will be fed to non-local spatial propagation module[34] to compute the final completed depth D .

3.5. Loss Fuction

We train our network by supervising all the outputs of each UFFM. First, we downsample G through average pooling to obtain multi-scale ground truths dense depth maps $\{g^n\}_{n=0}^N$ and use Eq. (1) to compute pseudo uncertainty. Then, we use \mathcal{L}_1 loss to supervise the predicted uncertainty and \mathcal{L}_2 loss for depth at each scale, which is described by Eq. (3).

$$\begin{aligned} L_g^n &= 0.5|u_g^n - \hat{u}_g^n| + \|d_g^n - g^n\| \\ L_l^n &= 0.5|u_l^n - \hat{u}_l^n| + \|d_l^n - g^n\| \\ L^n &= 0.5|u^n - \hat{u}^n| + \|d^n - g^n\| \\ L_{rec}^n &= 0.5(L_g^n + L_l^n) + L^n \end{aligned} \quad (3)$$

Then, we need to supervise the output of SFFM and non-local spatial propagation module, the overall loss function can be formulated by Eq. (4)

$$L = \sum_{n=0}^N \gamma^n L_{rec}^n + 0.05\|D' - G\| + \|D - G\| + \|D - G\| \quad (4)$$

where γ denotes the exponential decay factor, we set it as 0.8 in this paper to make the network pay more attention to the high-resolution outputs.

4. Experiments

4.1. Experimental Settings

In our experiments, we included both indoor and outdoor datasets.

NYU Depth V2. The NYU Depth V2[32] is a widely used indoor dataset in depth completion, which contains 40,800 RGBD images captured by Microsoft Kinect with an original resolution of 640×480 . Each image and depth map should be down-sampled to 320×240 , then center-cropped to 304×228 . We follow the previous work[28] to divide the dataset and set the upper bound of depth to 10 meters. Unlike previous methods that randomly sampled 500 points from the ground truth as sparse input, we sampled 5-500 random points during training.

SUN RGB-D The SUN RGB-D dataset[41] contains 10,335 raw RGB-D images captured by four different sensors. This dataset has more challenging scenes and sensors, which helps to evaluate model generalization efficiently.

KITTI depth completion. The KITTI dataset[9] contains over 93,000 raw sparse LIDAR scans (retrieved by Velodyne HDL-64E LiDAR sensor) and corresponding RGB images. The training, validation, and test set have 86,000, 7,000, and 1,000 samples, respectively[14], and the upper depth bound is 80 meters. For outdoor acquisition scenarios, in addition to high-emissivity objects and noise, the other factor is the different vertical resolution of the different sensors, e.g., 64-line LIDAR vs. 16-line LIDAR. So, we devised a simple but useful training strategy on KITTI

that randomly masks out all depths from 0%-95% of rows during training.

Evaluation metrics. We follow [13, 18] to use three metrics for the dense depth prediction evaluation **RMSE**: Root mean squared error, **MAE**: Mean absolute error, **REL**: Mean relative error. Performances using other metrics are reported in the Appendix.

Baselines. We compared SparseDC with several state-of-the-art depth completion networks, including NLSPN (ECCV 2020)[34], GraphCSPN (ECCV 2022)[25], CompletionFormer (CVPR 2023)[52], PENet (ICRA 2021)[15]. For a fair comparison, we retrained all of them using their code and our training strategy. Note that, we did not compare it with SpAgNet[5], SparseSPN[48] and some other state-of-the-art methods[22, 46, 51, 58], et al. because they did not release their code.

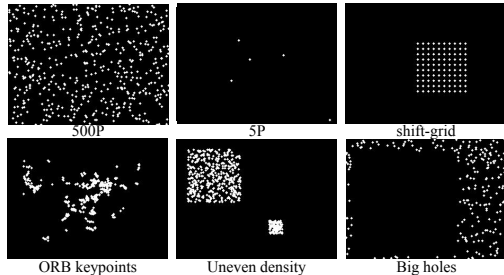


Figure 8. **Sparse depth patterns.** Including varying sparsity depth points, shift grid patterns (VCSEL TOF sensors), keypoints-based sampling, uneven density depth points, and big holes.

Implementation details. We trained our network with a batch size 16 for NYU (8 for each GPU) and 6 for KITTI (2 for each GPU) on the PyTorch platform, respectively. The Adam optimizer is used with an initial learning rate of 10^{-4} , which is decreased in every unimproved five epochs by a decay rate of 0.3. Our training process will stop when there is no improvement for ten consecutive epochs. We will release the source code and the trained models upon acceptance.

4.2. Results on NYU Depth V2

Unlike existing methods, which mainly focus on sparse-to-dense solutions, our networks pay more attention to dealing with sparse and non-uniform inputs. We trained our network on NYU Depth V2, and randomly sampled 5 ~ 500 depth points as inputs during training. SpAgNet[5] has proved that existing methods trained on fixed spatial patterns(500 random samples) are not comparable in the face of some challenging cases. For example, with only 5 points, the RMSE by NLSPN[34] is **1.033m**. So, we retrained the comparison methods using their released code and the same training strategy with us for a fair comparison.

We designed the following scenarios during testing to simulate varying sparsity and non-uniform inputs as shown in Fig. 8. 1) Varying sparsity inputs: Randomly sampling

Model	Samples	RMSE (m)↓	REL↓
NLSPN[34]	500	0.0984	0.0136
GraphCSPN[25]	500	0.0990	0.0136
CompletionFormer[52]	500	0.0984	0.0135
Ours	500	0.0976	0.0128
NLSPN[34]	200	0.1336	0.0201
GraphCSPN[25]	200	0.1338	0.0197
CompletionFormer[52]	200	0.1349	0.0205
Ours	200	0.1346	0.0191
NLSPN[34]	50	0.2123	0.0382
GraphCSPN[25]	50	0.2119	0.0375
CompletionFormer[52]	50	0.2183	0.0405
Ours	50	0.2079	0.0350
NLSPN[34]	10	0.3639	0.0827
GraphCSPN[25]	10	0.3650	0.0832
CompletionFormer[52]	10	0.3642	0.0874
Ours	10	0.3226	0.0681
NLSPN[34]	5	0.4439	0.1094
GraphCSPN[25]	5	0.4555	0.1151
CompletionFormer[52]	5	0.4377	0.1144
Ours	5	0.3816	0.0877
NLSPN[34]	shift_grid	0.4263	0.1043
GraphCSPN[25]	shift_grid	0.4485	0.1083
CompletionFormer[52]	shift_grid	0.4313	0.1149
Ours	shift_grid	0.3736	0.0852
NLSPN[34]	uneven density	0.3931	0.0909
GraphCSPN[25]	uneven density	0.3991	0.0920
CompletionFormer[52]	uneven density	0.3919	0.0961
Ours	uneven density	0.3543	0.0763
NLSPN[34]	ORB keypoint	0.2590	0.0625
GraphCSPN[25]	ORB keypoint	0.2571	0.0603
CompletionFormer[52]	ORB keypoint	0.2660	0.0672
Ours	ORB keypoint	0.2441	0.0541
NLSPN[34]	big holes	0.2368	0.0402
GraphCSPN[25]	big holes	0.2443	0.0403
CompletionFormer[52]	big holes	0.2493	0.0434
Ours	big holes	0.2262	0.0362

Table 1. **Results on NYU Depth V2 with different patterns.** Quantitative comparisons with state-of-the-art methods in different spatial patterns. The best results are red and in bold.

depth points included some extreme cases, such as only 5 valid depth points. 2) VCSEL TOF sensors[27]: Sampling a shifting grid from the ground truth. 3) Uneven density: Randomly selected two regions with different sizes and different numbers of depth points from the ground truth. 4) Keypoint-based Sampling: Following the SpaseSPN[48], we use a keypoints-based(ORB[39]) sample strategy to simulate the sparse depth values available from keypoint triangulation. 5) Holes: Randomly select depth points, then select a 200×200 square grid, and remove all depth points inside the grid.

The quantitative comparison results on NYU Depth V2 under various non-uniform settings are shown in Tab. 7 and some visual comparisons are given in Fig. 9. It can be seen that SparseDC consistently outperforms the baselines only except the 200-sample case. Moreover, our

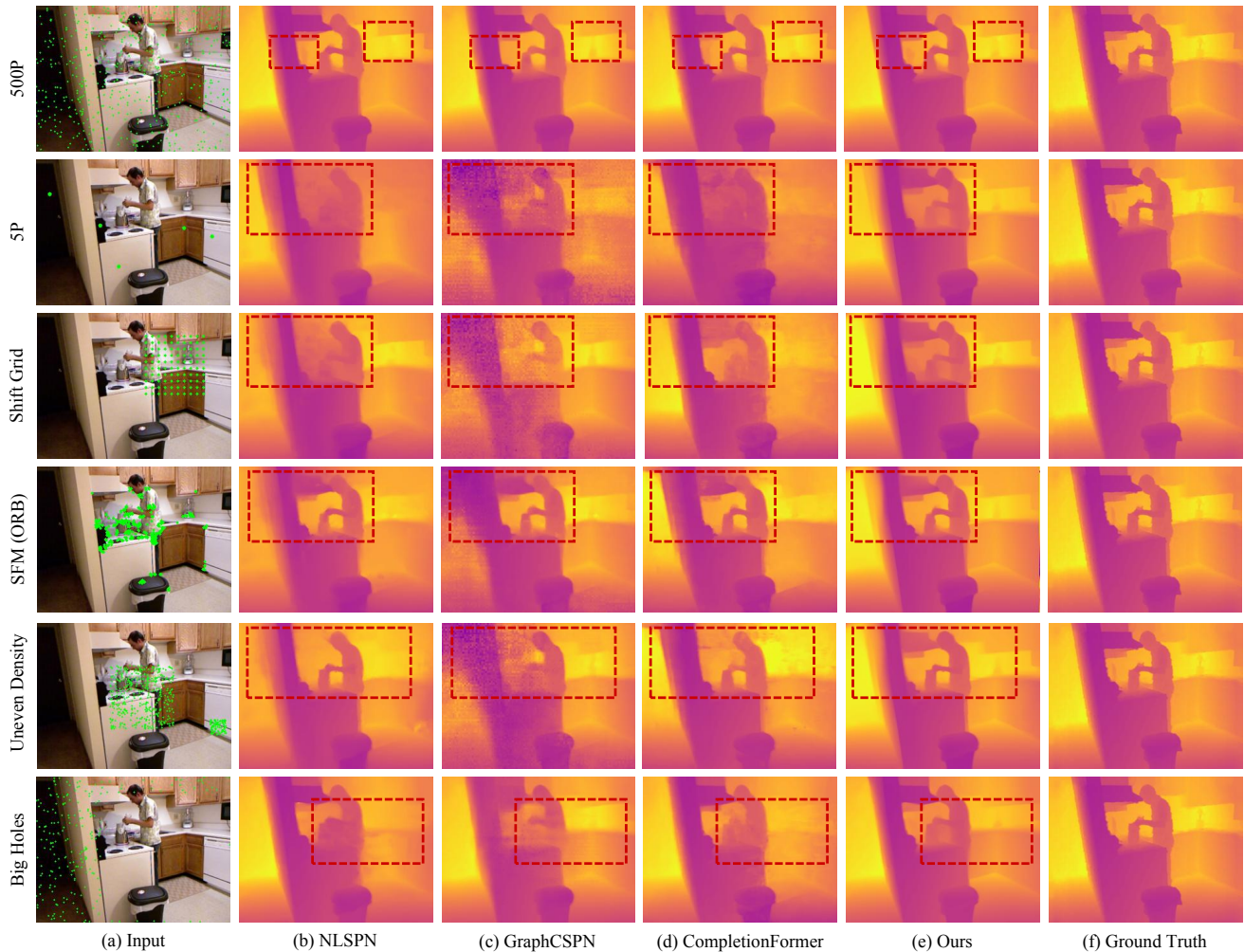


Figure 9. **Qualitative results on NYU Depth V2.** Comparing completion results with different patterns of inputs using different methods.

method achieved 17% improvements on REL and 7.8% improvements on RMSE, respectively, over the State-of-the-art method CompletionFormer[52]. This is mainly because SparseDC can dynamically adjust the reliance on both local and global features during the depth completion process and thus can achieve a balance to retain the precise geometry of regions with available depth values and accurate structures in regions with no depth input.

4.3. Generalization results on SUN RGB-D

To validate the generalization ability of our method, we use the model trained on NYU[32] to conduct depth completion on SUN RGB-D directly. In the test set, we used the noisy and incomplete raw depth image as the input without sampling. As shown in Tab. 2, our proposed SparseDC performs best in most metrics. The augment-based strategy makes [25, 34] overfit the training data. Completionformer[52] and SparseDC fuse global and local information simulta-

Methods	Params	RMSE(m)↓	REL↓
NLSPN[34]	25.8M	0.5966	0.1257
NLSPN*[34]	25.8M	3.5966	1.9789
GraphCSPN*[25]	26M	4.3420	2.2700
CompletionFormer[52]	45M	0.9613	0.4707
CompletionFormer*[52]	45M	0.6047	0.1574
Ours	38.2M	0.4536	0.1180

Table 2. **Generalization Ability Test on SUN RGBD.** * denotes trained model using our training strategy, without * is their released pretrained model trained using fixed patterns.

neously, resulting in improvements and robustness with unseen patterns. We report the corresponding visual comparison results in the Appendix.

4.4. Results on KITTI Depth Completion

On the outdoor KITTI dataset, we randomly mask some rows in depth maps during training as mentioned in Sec. 4.1.

Methods	Scanning Lines	RMSE(m)↓	MAE(m)↓
NLSPN[34]	lines4	2.2648	0.7492
PENet[15]	lines4	2.2323	0.8132
CompletionFormer[52]	lines4	2.1500	0.7401
DySPN[22]	lines4	2.2858	0.8343
Ours	lines4	2.1029	0.7012
NLSPN[34]	lines8	1.5452	0.4593
PENet[15]	lines8	1.5983	0.5261
Ours	lines8	1.5286	0.4444
NLSPN[34]	lines16	1.1781	0.3274
PENet[15]	lines16	1.2231	0.3818
CompletionFormer[52]	lines16	1.2186	0.3374
DySPN[22]	lines16	1.2748	0.3664
Ours	lines16	1.1764	0.3178
NLSPN[34]	lines32	0.9575	0.2587
PENet[15]	lines32	0.9866	0.3019
Ours	lines32	0.9485	0.2488
NLSPN[34]	lines64	0.8125	0.2167
PENet[15]	lines64	0.8406	0.2472
CompletionFormer[52]	lines64	0.8487	0.2159
DySPN[22]	lines64	0.8785	0.2286
Ours	lines64	0.7966	0.2051

Table 3. **Results on KITTI DC.** Quantitative comparisons with state-of-the-art methods on varying scanning lines.

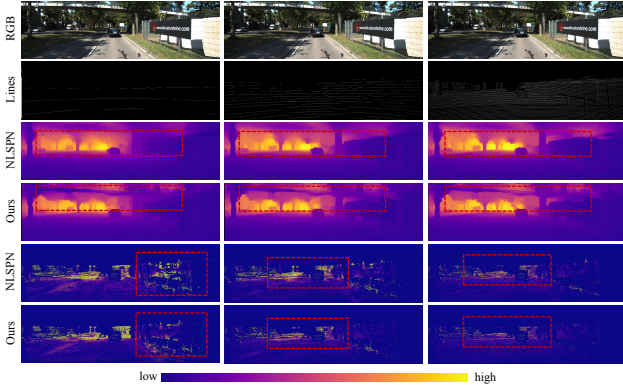


Figure 10. **Qualitative results on KITTI DC.** We report the completed depth and error map with varying scanning lines as inputs.

Due to resource constraints, we directly use the metric in reported CompletionFormer[52]. The specific results are shown in Tab. 3. It can be seen that SparseDC consistently outperforms the baselines by a large margin in MAE, and the gap becomes larger when fewer scanning lines are kept, demonstrating the effectiveness of SparseDC under sparse input.

4.5. Ablation Study

To demonstrate the effectiveness of each component proposed in SparseDC, we conducted corresponding ablation experiments on NYU Depth V2 dataset by removing each component as follows.

- Remove the Sparse Feature Filling Module, and replace it with two simple convolution layers, as previous

Model	samples	RMSE(m)↓	REL↓
w/o UFFM	500	0.0973	0.0128
w/o SFFM	500	0.0974	0.0128
w/o Two-Branch	500	0.0984	0.0136
Full Model	500	0.0976	0.0128
w/o UFFM	50	0.2089	0.0356
w/o SFFM	50	0.2092	0.0354
w/o Two-Branch	50	0.2123	0.0382
Full Model	50	0.2079	0.0350
w/o UFFM	5	0.3846	0.0904
w/o SFFM	5	0.3854	0.0918
w/o Two-Branch	5	0.4439	0.1094
Full Model	5	0.3816	0.0877
w/o UFFM	shift_grid	0.4618	0.1072
w/o SFFM	shift_grid	0.4380	0.1042
w/o Two-Branch	shift_grid	0.4263	0.1043
Full Model	shift_grid	0.3736	0.0852
w/o UFFM	uneven density	0.5391	0.1266
w/o SFFM	uneven density	0.4124	0.0934
w/o Two-Branch	uneven density	0.3931	0.0909
Full Model	uneven density	0.3543	0.0763

Table 4. **Ablation study.** The evaluation results of different components of SparseDC.

methods[25, 34].

- Remove the Uncertainty-Guide Feature Fusion Module, and use Eq. (5) to fuse the extracted features.

$$f^n = Gate(f_l^n \oplus \cdot f_g^n) \quad (5)$$

- Removing the two-branch feature extraction structure in favor of a single-branch one, i.e., the overall model will degenerate into a combination of ResNet[12] with a non-local spatial propagation module, so we use the retrained NLSPN[34] as a replacement.

All ablation models are trained under the same settings as SparseDC, the results are shown in Tab. 4.

Our full pipeline gets the minimum RMSE and REL value for most experiments, removing any component will degrade the overall performance of the network. In addition, the results show that removing the Two-Branch feature extraction structure has the greatest impact on the network in the face of extremely sparse inputs. This is because the Two-Branch structure provides both global semantic and local geometric information, which is necessary for dealing with non-uniform inputs. Furthermore, SFFM provides a stabilized feature space for sparse depth maps, which makes the depth estimated by the network more accurate. UFFM can predict the uncertainty based on the spatial pattern of the inputs, and then explicitly guides the fusion process of features from different branches by this uncertainty, as shown in Fig. 6. Both modules benefit SparseDC with sparse and non-uniform input.

5. Conclusion

This paper focused on depth completion of *sparse* and *non-uniform* inputs. To address this, We first propose an SFFM module to improve the feature stability by explicitly filling the unstable depth features with stable image features. Then, we introduce a two-branch feature embedder to extract local or long-term information of the input depth map and RGB image by CNNs and ViTs. Here we propose an uncertainty-based fusion module called UFFM to predict both precise local geometries of regions with available depth values and accurate structures in regions with no depth input. Extensive indoor and outdoor experiments demonstrate our method’s effectiveness when facing sparse and non-uniform inputs.

References

- [1] Abien Fred Agarap. Deep learning using rectified linear units (relu). *arXiv preprint arXiv:1803.08375*, 2018. 4
- [2] Gerardo Atanacio-Jiménez, José-Joel González-Barbosa, Juan B Hurtado-Ramos, Francisco J Ornelas-Rodríguez, Hugo Jiménez-Hernández, Teresa García-Ramirez, and Ricardo González-Barbosa. Lidar velodyne hdl-64e calibration using pattern planes. *International Journal of Advanced Robotic Systems*, 8(5):59, 2011. 2
- [3] Xinjing Cheng, Peng Wang, and Ruigang Yang. Depth Estimation via Affinity Learned with Convolutional Spatial Propagation Network. In *Computer Vision – ECCV 2018*, pages 108–125. Springer International Publishing, Cham, 2018. 3
- [4] Xinjing Cheng, Peng Wang, Chenye Guan, and Ruigang Yang. CSPN++: Learning Context and Resource Aware Convolutional Spatial Propagation Networks for Depth Completion, 2019. 3
- [5] Andrea Conti, Matteo Poggi, and Stefano Mattoccia. Sparsity agnostic depth completion. In *Proceedings of the IEEE/CVF Winter Conference on Applications of Computer Vision*, pages 5871–5880, 2023. 3, 6
- [6] Spconv Contributors. Spconv: Spatially sparse convolution library. <https://github.com/traveller59/spconv>, 2022. 2
- [7] Marius Cordts, Mohamed Omran, Sebastian Ramos, Timo Rehfeld, Markus Enzweiler, Rodrigo Benenson, Uwe Franke, Stefan Roth, and Bernt Schiele. The cityscapes dataset for semantic urban scene understanding. In *Proceedings of the IEEE conference on computer vision and pattern recognition*, pages 3213–3223, 2016. 1
- [8] Andreas Geiger, Julius Ziegler, and Christoph Stiller. Stereoscan: Dense 3d reconstruction in real-time. In *2011 IEEE intelligent vehicles symposium (IV)*, pages 963–968. Ieee, 2011. 1
- [9] Andreas Geiger, Philip Lenz, and Raquel Urtasun. Are we ready for autonomous driving? the kitti vision benchmark suite. In *Conference on Computer Vision and Pattern Recognition (CVPR)*, 2012. 2, 3, 5
- [10] Benjamin Graham and Laurens Van der Maaten. Sub-manifold sparse convolutional networks. *arXiv preprint arXiv:1706.01307*, 2017. 2
- [11] Jiaqi Gu, Zhiyu Xiang, Yuwen Ye, and Lingxuan Wang. DenseLiDAR: A Real-Time Pseudo Dense Depth Guided Depth Completion Network. *IEEE Robotics and Automation Letters*, 6(2):1808–1815, 2021. 3
- [12] Kaiming He, Xiangyu Zhang, Shaoqing Ren, and Jian Sun. Deep residual learning for image recognition. In *Proceedings of the IEEE conference on computer vision and pattern recognition*, pages 770–778, 2016. 2, 4, 8
- [13] Junjie Hu, Mete Ozay, Yan Zhang, and Takayuki Okatani. Revisiting single image depth estimation: Toward higher resolution maps with accurate object boundaries. In *2019 IEEE winter conference on applications of computer vision (WACV)*, pages 1043–1051. IEEE, 2019. 6
- [14] Junjie Hu, Chenyu Bao, Mete Ozay, Chenyou Fan, Qing Gao, Honghai Liu, and Tin Lun Lam. Deep Depth Completion from Extremely Sparse Data: A Survey. *IEEE Transactions on Pattern Analysis and Machine Intelligence*, 2023. 3, 5
- [15] Mu Hu, Shuling Wang, Bin Li, Shiyu Ning, Li Fan, and Xiaojin Gong. PENet: Towards Precise and Efficient Image Guided Depth Completion, 2021. 6, 8
- [16] Sergey Ioffe and Christian Szegedy. Batch normalization: Accelerating deep network training by reducing internal covariate shift. In *International conference on machine learning*, pages 448–456. pmlr, 2015. 4
- [17] Yurim Jeon, Hwchang Kim, and Seung-Woo Seo. ABCD: Attentive Bilateral Convolutional Network for Robust Depth Completion. *IEEE Robotics and Automation Letters*, 7(1): 81–87, 2022. 3
- [18] Hualie Jiang, Laiyan Ding, Junjie Hu, and Rui Huang. Plnet: Plane and line priors for unsupervised indoor depth estimation. In *2021 International Conference on 3D Vision (3DV)*, pages 741–750. IEEE, 2021. 6
- [19] Leonid Keselman, John Iselin Woodfill, Anders Grunnet-Jepsen, and Achintya Bhowmik. Intel realsense stereoscopic depth cameras. In *Proceedings of the IEEE conference on computer vision and pattern recognition workshops*, pages 1–10, 2017. 1
- [20] Alex Krizhevsky, Ilya Sutskever, and Geoffrey E Hinton. Imagenet classification with deep convolutional neural networks. *Advances in neural information processing systems*, 25, 2012. 4
- [21] Li-Jia Li, Richard Socher, and Li Fei-Fei. Towards total scene understanding: Classification, annotation and segmentation in an automatic framework. In *2009 IEEE Conference on Computer Vision and Pattern Recognition*, pages 2036–2043. IEEE, 2009. 1
- [22] Yuankai Lin, Tao Cheng, Qi Zhong, Wending Zhou, and Hua Yang. Dynamic Spatial Propagation Network for Depth Completion. *Proceedings of the AAAI Conference on Artificial Intelligence*, 36(2):1638–1646, 2022. 3, 6, 8, 1
- [23] Lina Liu, Xibin Song, Xiaoyang Lyu, Junwei Diao, Mengmeng Wang, Yong Liu, and Liangjun Zhang. FCFR-Net: Feature Fusion based Coarse-to-Fine Residual Learning for Depth Completion. page 9, 2020. 3

- [24] Lina Liu, Yiyi Liao, Yue Wang, Andreas Geiger, and Yong Liu. Learning Steering Kernels for Guided Depth Completion. *IEEE Transactions on Image Processing*, 30:2850–2861, 2021. [3](#)
- [25] Xin Liu, Xiaofei Shao, Bo Wang, Yali Li, and Shengjin Wang. GraphCSPN: Geometry-Aware Depth Completion via Dynamic GCNs, 2022. [3](#), [6](#), [7](#), [8](#), [1](#), [2](#)
- [26] Chen Long, WenXiao Zhang, Ruihui Li, Hao Wang, Zhen Dong, and Bisheng Yang. Pc2-pu: Patch correlation and point correlation for effective point cloud upsampling. In *Proceedings of the 30th ACM International Conference on Multimedia*, pages 2191–2201, 2022. [1](#)
- [27] Gregor Luetzenburg, Aart Kroon, and Anders A Bjørk. Evaluation of the apple iphone 12 pro lidar for an application in geosciences. *Scientific reports*, 11(1):22221, 2021. [6](#)
- [28] Fangchang Ma and Sertac Karaman. Sparse-to-dense: Depth prediction from sparse depth samples and a single image. In *2018 IEEE international conference on robotics and automation (ICRA)*, pages 4796–4803. IEEE, 2018. [3](#), [5](#)
- [29] Markus Maurer, J Christian Gerdes, Barbara Lenz, and Hermann Winner. *Autonomous driving: technical, legal and social aspects*. Springer Nature, 2016. [1](#)
- [30] Nando Metzger, Rodrigo Caye Daudt, and Konrad Schindler. Guided Depth Super-Resolution by Deep Anisotropic Diffusion, 2022. [3](#)
- [31] Fabian Märkert, Martin Sunkel, Anselm Haselhoff, and Stefan Rudolph. Segmentation-guided Domain Adaptation for Efficient Depth Completion, 2022. [3](#)
- [32] Pushmeet Kohli Nathan Silberman, Derek Hoiem and Rob Fergus. Indoor segmentation and support inference from rgbd images. In *ECCV*, 2012. [2](#), [3](#), [5](#), [7](#)
- [33] Hailong Pan, Tao Guan, Yawei Luo, Liya Duan, Yuan Tian, Liu Yi, Yizhu Zhao, and Junqing Yu. Dense 3d reconstruction combining depth and rgb information. *Neurocomputing*, 175:644–651, 2016. [1](#)
- [34] Jinsun Park, Kyungdon Joo, Zhe Hu, Chi-Kuei Liu, and In So Kweon. Non-local Spatial Propagation Network for Depth Completion. In *Computer Vision – ECCV 2020*, pages 120–136. Springer International Publishing, Cham, 2020. [3](#), [4](#), [5](#), [6](#), [7](#), [8](#), [1](#), [2](#)
- [35] Mi Jin Park, Dong Jun Kim, Unjoo Lee, Eun Jin Na, and Hong Jin Jeon. A literature overview of virtual reality (vr) in treatment of psychiatric disorders: recent advances and limitations. *Frontiers in psychiatry*, 10:505, 2019. [1](#)
- [36] Jiexiong Qiu, Zhaopeng Cui, Yinda Zhang, Xingdi Zhang, Shuaicheng Liu, Bing Zeng, and Marc Pollefeys. Deeplidar: Deep surface normal guided depth prediction for outdoor scene from sparse lidar data and single color image. In *Proceedings of the IEEE/CVF Conference on Computer Vision and Pattern Recognition*, pages 3313–3322, 2019. [3](#)
- [37] Kyeongha Rho, Jinsung Ha, and Youngjung Kim. GuideFormer: Transformers for Image Guided Depth Completion. page 10, 2020. [3](#)
- [38] Olaf Ronneberger, Philipp Fischer, and Thomas Brox. U-net: Convolutional networks for biomedical image segmentation. In *Medical Image Computing and Computer-Assisted Intervention–MICCAI 2015: 18th International Conference, Munich, Germany, October 5-9, 2015, Proceedings, Part III 18*, pages 234–241. Springer, 2015. [4](#)
- [39] Ethan Rublee, Vincent Rabaud, Kurt Konolige, and Gary Bradski. Orb: An efficient alternative to sift or surf. In *2011 International conference on computer vision*, pages 2564–2571. Ieee, 2011. [6](#)
- [40] Shuwei Shao, Zhongcai Pei, Weihai Chen, Ran Li, Zhong Liu, and Zhengguo Li. Urcdc-depth: Uncertainty rectified cross-distillation with cutflip for monocular depth estimation. *arXiv preprint arXiv:2302.08149*, 2023. [5](#)
- [41] Shuran Song, Samuel P Lichtenberg, and Jianxiong Xiao. Sun rgb-d: A rgb-d scene understanding benchmark suite. In *Proceedings of the IEEE conference on computer vision and pattern recognition*, pages 567–576, 2015. [3](#), [5](#), [2](#)
- [42] Jie Tang, Fei-Peng Tian, Wei Feng, Jian Li, and Ping Tan. Learning Guided Convolutional Network for Depth Completion, 2019. [1](#)
- [43] Jonas Uhrig, Nick Schneider, Lukas Schneider, Uwe Franke, Thomas Brox, and Andreas Geiger. Sparsity invariant cnns. In *2017 international conference on 3D Vision (3DV)*, pages 11–20. IEEE, 2017. [2](#), [3](#)
- [44] Wenhai Wang, Enze Xie, Xiang Li, Deng-Ping Fan, Kaitao Song, Ding Liang, Tong Lu, Ping Luo, and Ling Shao. Pyramid vision transformer: A versatile backbone for dense prediction without convolutions. In *Proceedings of the IEEE/CVF international conference on computer vision*, pages 568–578, 2021. [2](#)
- [45] Wenhai Wang, Enze Xie, Xiang Li, Deng-Ping Fan, Kaitao Song, Ding Liang, Tong Lu, Ping Luo, and Ling Shao. Pvtv2: Improved baselines with pyramid vision transformer. *Computational Visual Media*, 8(3):1–10, 2022. [2](#), [4](#)
- [46] Yufei Wang, Bo Li, Ge Zhang, Qi Liu, Tao Gao, and Yuchao Dai. Lrru: Long-short range recurrent updating networks for depth completion. In *Proceedings of the IEEE/CVF International Conference on Computer Vision*, pages 9422–9432, 2023. [2](#), [3](#), [6](#)
- [47] Sanghyun Woo, Shoubhik Debnath, Ronghang Hu, Xinlei Chen, Zhuang Liu, In So Kweon, and Saining Xie. Convnext v2: Co-designing and scaling convnets with masked autoencoders. In *Proceedings of the IEEE/CVF Conference on Computer Vision and Pattern Recognition*, pages 16133–16142, 2023. [2](#), [4](#)
- [48] Yuqun Wu, Jae Yong Lee, and Derek Hoiem. Sparse spn: Depth completion from sparse keypoints. *arXiv preprint arXiv:2212.00987*, 2022. [3](#), [6](#)
- [49] Jin Xu, Zishan Li, Bowen Du, Miaomiao Zhang, and Jing Liu. Reluplex made more practical: Leaky relu. In *2020 IEEE Symposium on Computers and Communications (ISCC)*, pages 1–7. IEEE, 2020. [4](#)
- [50] Yan Xu, Xinge Zhu, Jianping Shi, Guofeng Zhang, Hujun Bao, and Hongsheng Li. Depth completion from sparse lidar data with depth-normal constraints. In *Proceedings of the IEEE/CVF International Conference on Computer Vision*, pages 2811–2820, 2019. [3](#)
- [51] Zhiqiang Yan, Kun Wang, Xiang Li, Zhenyu Zhang, Jun Li, and Jian Yang. RigNet: Repetitive Image Guided Network for Depth Completion, 2022. [2](#), [3](#), [6](#)

- [52] Zhang Youmin, Guo Xianda, Poggi Matteo, Zhu Zheng, Huang Guan, and Mattocchia Stefano. CompletionFormer: Depth Completion with Convolutions and Vision Transformers, 2023. [2](#), [3](#), [6](#), [7](#), [8](#), [1](#)
- [53] Jiahui Yu, Zhe Lin, Jimei Yang, Xiaohui Shen, Xin Lu, and Thomas S Huang. Free-form image inpainting with gated convolution. In *Proceedings of the IEEE/CVF international conference on computer vision*, pages 4471–4480, 2019. [4](#)
- [54] Steve Chi-Yin Yuen, Gallayanee Yaoyuneyong, and Erik Johnson. Augmented reality: An overview and five directions for ar in education. *Journal of Educational Technology Development and Exchange (JETDE)*, 4(1):11, 2011. [1](#)
- [55] Ekim Yurtsever, Jacob Lambert, Alexander Carballo, and Kazuya Takeda. A survey of autonomous driving: Common practices and emerging technologies. *IEEE access*, 8:58443–58469, 2020. [1](#)
- [56] Zhengyou Zhang. Microsoft kinect sensor and its effect. *IEEE multimedia*, 19(2):4–10, 2012. [1](#)
- [57] Shanshan Zhao, Mingming Gong, Huan Fu, and Dacheng Tao. Adaptive Context-Aware Multi-Modal Network for Depth Completion. *IEEE Transactions on Image Processing*, 30:5264–5276, 2021. [3](#)
- [58] Wending Zhou, Xu Yan, Yinghong Liao, Yuankai Lin, Jin Huang, Gangming Zhao, Shuguang Cui, and Zhen Li. BEV@ DC: Bird’s-Eye View Assisted Training for Depth Completion. In *Proceedings of the IEEE/CVF Conference on Computer Vision and Pattern Recognition*, pages 9233–9242, 2023. [2](#), [3](#), [6](#)

SparseDC: Depth Completion from sparse and non-uniform inputs

Supplementary Material

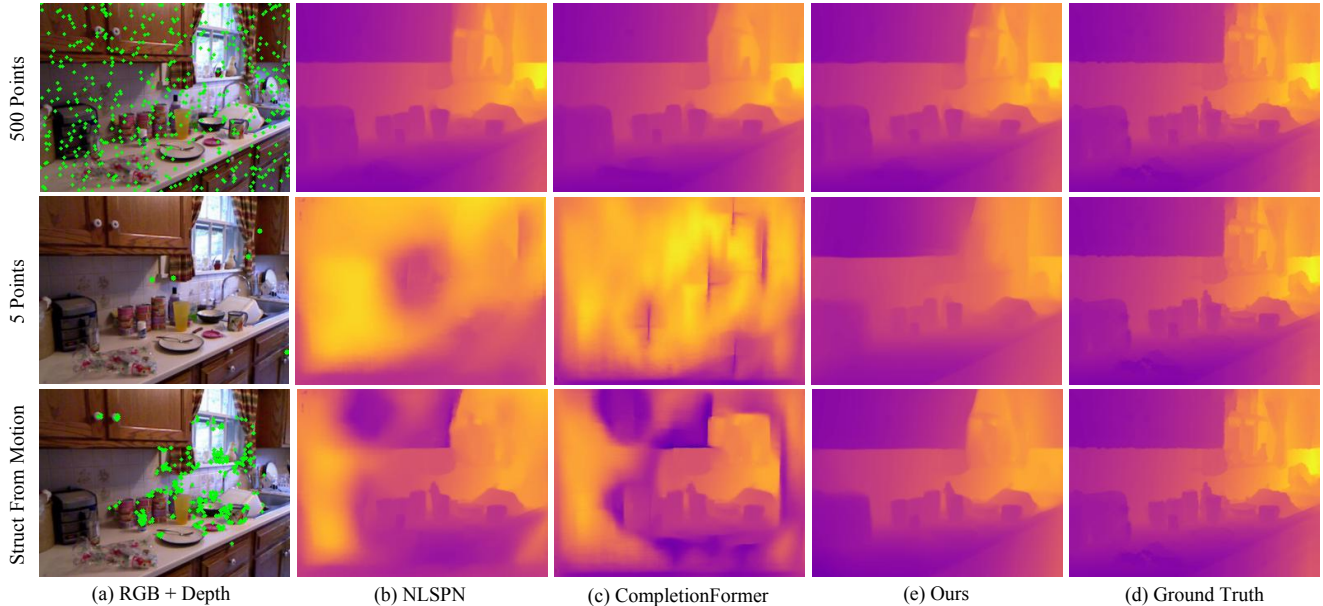


Figure 11. **Qualitative results on NYU Depth V2.** Comparing completion results with different patterns of inputs using different methods trained in fixed distribution.

6. Appendix

In the following, we show additional experimental results.

6.1. More results on NYU Depth V2

We trained the comparison methods using their released code and the same training strategy with us (described in Sec. 4.1), because the existing methods trained on fixed spatial patterns (500 random samples) are not comparable in the face of some challenging cases. To prove this point, we report the results of their pre-trained models in Tab. 5. The

Model	Samples	RMSE(m)↓	REL↓
NLSPN[34]	500	0.0917	0.0116
CompletionFormer[52]	500	0.0901	0.0119
Ours	500	0.0976	0.0128
NLSPN[34]	5	1.0389	0.2647
CompletionFormer[52]	5	1.1405	0.3073
Ours	5	0.3816	0.0877
NLSPN[34]	ORB keypoint	0.5997	0.1462
CompletionFormer[52]	ORB keypoint	0.6222	0.2222
Ours	ORB keypoint	0.2441	0.0541

Table 5. **Results on NYU Depth V2.** Quantitative comparisons with the state-of-the-art methods trained in fixed distribution. The best results are red and in bold.

Methods	Params	RMSE(m)↓	REL↓
GuideNet[42]	74M	0.101	0.015
DySPN[22]	26M	0.090	0.012
NLSPN[34]	25.8M	0.092	0.012
GraphCSPN[25]	26M	0.090	0.012
CompletionFormer[52]	45M	0.090	0.012
Ours	38.2M	0.093	0.012

Table 6. **Results on NYU Depth V2 with fixed distribution.** Quantitative comparisons with state-of-the-art methods in a fixed spatial pattern.

visualization results in Fig. 11 also illustrate that the existing methods cannot reconstruct the overall scene structure when dealing with such challenging cases.

Furthermore, we validated the performance of our method with a fixed distribution. We used 500 sampling random depth points as inputs and retrained our model, like the previous setting. Even though SparseDC is focused on depth completion from *sparse and non-uniform* inputs, our method still exhibits comparable performance as shown in the Tab. 6.

Finally, we report the performance of comparison methods using other metrics in Tab. 7, and show more visualizations in Fig. 12.

Methods	Samples	RMSE (m)↓	MAE (m)↓	IRMSE ($\frac{1}{m}$)↓	iMAE ($\frac{1}{m}$)↓	REL ↓	$\delta_{1.25} \uparrow$	$\delta_{1.25}^2 \uparrow$	$\delta_{1.25}^3 \uparrow$
NLSPN[34]	500	0.0984	0.0395	0.0153	0.0058	0.0136	0.9949	0.9992	0.9998
GraphCSPN[25]	500	0.0990	0.0399	0.0153	0.0059	0.0136	0.9948	0.9992	0.9998
CompletionFormer[52]	500	0.0984	0.0392	0.0153	0.0058	0.0135	0.9948	0.9992	0.9998
Ours	500	0.0976	0.0379	0.0148	0.0054	0.0128	0.9949	0.9992	0.9998
NLSPN[34]	200	0.1336	0.0579	0.0209	0.0087	0.0201	0.9902	0.9983	0.9996
GraphCSPN[25]	200	0.1338	0.0575	0.0207	0.0085	0.0197	0.9902	0.9982	0.9995
CompletionFormer[52]	200	0.1349	0.0588	0.0214	0.0089	0.0205	0.9898	0.9982	0.9995
Ours	200	0.1346	0.0565	0.0203	0.0081	0.0191	0.9899	0.9982	0.9995
NLSPN[34]	50	0.2123	0.1078	0.0345	0.0168	0.0382	0.9743	0.9948	0.9986
GraphCSPN[25]	50	0.2119	0.1069	0.0340	0.0165	0.0375	0.9745	0.9942	0.9984
CompletionFormer[52]	50	0.2183	0.1124	0.0362	0.0178	0.0405	0.9717	0.9941	0.9984
Ours	50	0.2079	0.1017	0.0323	0.0152	0.0350	0.9755	0.9946	0.9985
NLSPN[34]	10	0.3639	0.2254	0.0624	0.0373	0.0827	0.9154	0.9810	0.9950
GraphCSPN[25]	10	0.3650	0.2237	0.0639	0.0373	0.0832	0.9138	0.9796	0.9943
CompletionFormer[52]	10	0.3642	0.2300	0.0650	0.0387	0.0874	0.9110	0.9802	0.9946
Ours	10	0.3226	0.1923	0.0536	0.0308	0.0681	0.9358	0.9854	0.9960
NLSPN[34]	5	0.4439	0.2953	0.0770	0.0497	0.1094	0.8674	0.9696	0.9925
GraphCSPN[25]	5	0.4555	0.3001	0.0814	0.0512	0.1151	0.8604	0.9650	0.9899
CompletionFormer[52]	5	0.4377	0.2961	0.0791	0.0507	0.1144	0.8657	0.9683	0.9917
Ours	5	0.3816	0.2456	0.0649	0.0405	0.0877	0.9059	0.9795	0.9945
NLSPN[34]	shift_grid	0.4263	0.2718	0.0791	0.0487	0.1043	0.8655	0.9671	0.9923
GraphCSPN[25]	shift_grid	0.4485	0.2808	0.0833	0.0502	0.1083	0.8531	0.9614	0.9899
CompletionFormer[52]	shift_grid	0.4313	0.2812	0.0834	0.0512	0.1149	0.8560	0.9635	0.9901
Ours	shift_grid	0.3736	0.2331	0.0680	0.0409	0.0852	0.8987	0.9782	0.9947
NLSPN[34]	uneven density	0.3931	0.2438	0.0710	0.0425	0.0909	0.8901	0.9741	0.9935
GraphCSPN[25]	uneven density	0.3991	0.2420	0.0737	0.0427	0.0920	0.8855	0.9705	0.9922
CompletionFormer[52]	uneven density	0.3919	0.2432	0.0724	0.0424	0.0961	0.8867	0.9719	0.9921
Ours	uneven density	0.3543	0.2141	0.0632	0.0372	0.0763	0.9121	0.9809	0.9950
NLSPN[34]	ORB keypoint	0.2590	0.1565	0.0542	0.0301	0.0625	0.9479	0.9890	0.9965
GraphCSPN[25]	ORB keypoint	0.2571	0.1510	0.0540	0.0290	0.0603	0.9481	0.9880	0.9961
CompletionFormer[52]	ORB keypoint	0.2660	0.1616	0.0576	0.0316	0.0672	0.9417	0.9873	0.9965
Ours	ORB keypoint	0.2441	0.1404	0.0498	0.0265	0.0541	0.9539	0.9898	0.9970
NLSPN[34]	big holes	0.2368	0.1205	0.0332	0.0171	0.0402	0.9695	0.9944	0.9986
GraphCSPN[25]	big holes	0.2443	0.1224	0.0336	0.0171	0.0403	0.9675	0.9932	0.9983
CompletionFormer[52]	big holes	0.2493	0.1273	0.0350	0.0180	0.0434	0.9648	0.9933	0.9983
Ours	big holes	0.2262	0.1121	0.0307	0.0155	0.0362	0.9731	0.9944	0.9985

Table 7. **Results on NYU Depth V2 in all Metrics.** Quantitative comparisons with state-of-the-art methods in different spatial patterns. The best results are red and in bold.

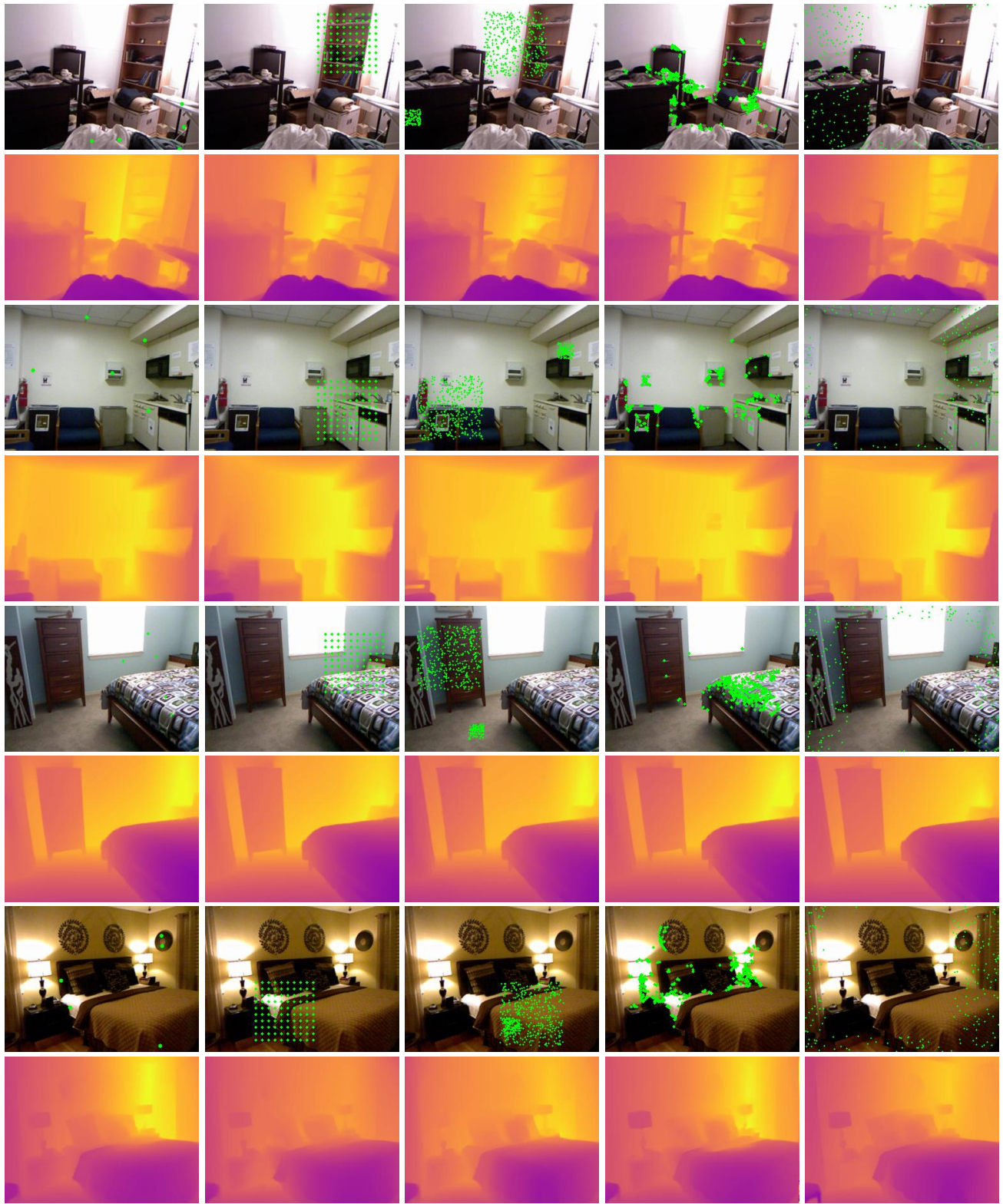
6.2. More results on KITTI

Fig. 13 shows, on an image of the KITTI DC dataset and three different depth inputs, the outcome of SparseDC. Our method can effectively maintain the overall scene structure under different lines of depth inputs.

6.3. More results on SUN RGB-D

SUN RGB-D[41] contains 10,355 RGB-D images captured by four different sensors. It was used to validate the generalization ability of our method. We used the noisy and incomplete raw depth data as inputs without sampling, and used the refined depth maps based on multiple frames as the ground truths for evaluation. The input images were resized to 320×240 and randomly cropped to 304×228 . The Qualitative comparison results are shown in Fig. 14. For

such challenging cases (noisy, incomplete, unseen), existing methods with or without augment-based strategy are difficult to obtain satisfactory results, whereas our method achieved the best performance due to its meticulous design.



5 P

Shift Grid

Uneven Density

SFM (ORB)

Big holes

Figure 12. **Qualitative results on NYU Depth V2.** Examples of using SparseDC to complete sparse depth with different patterns.

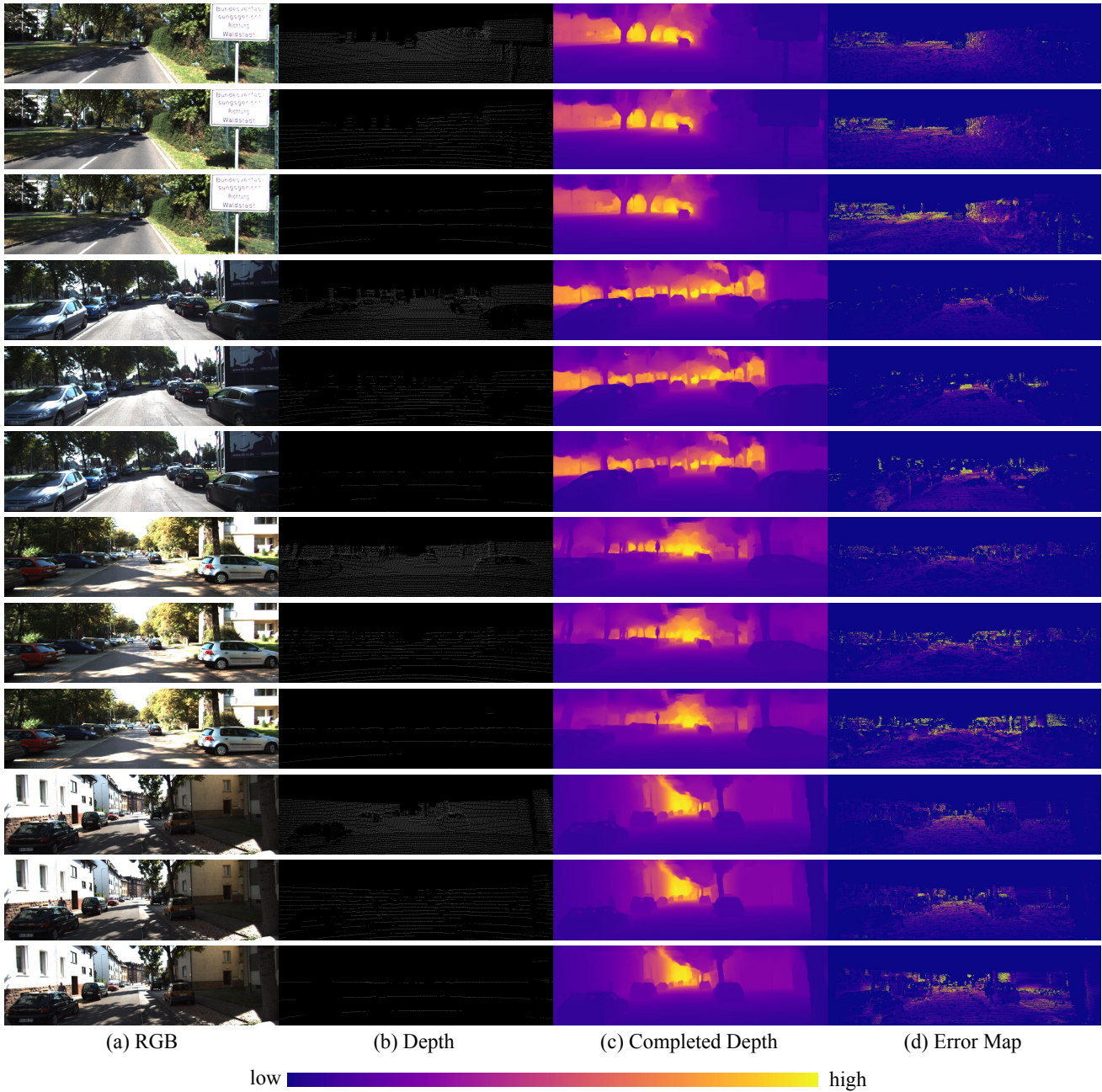


Figure 13. **Qualitative results on Kitti.** We report completed results from SparseDC with 4, 16, and 64 line depth inputs, respectively.

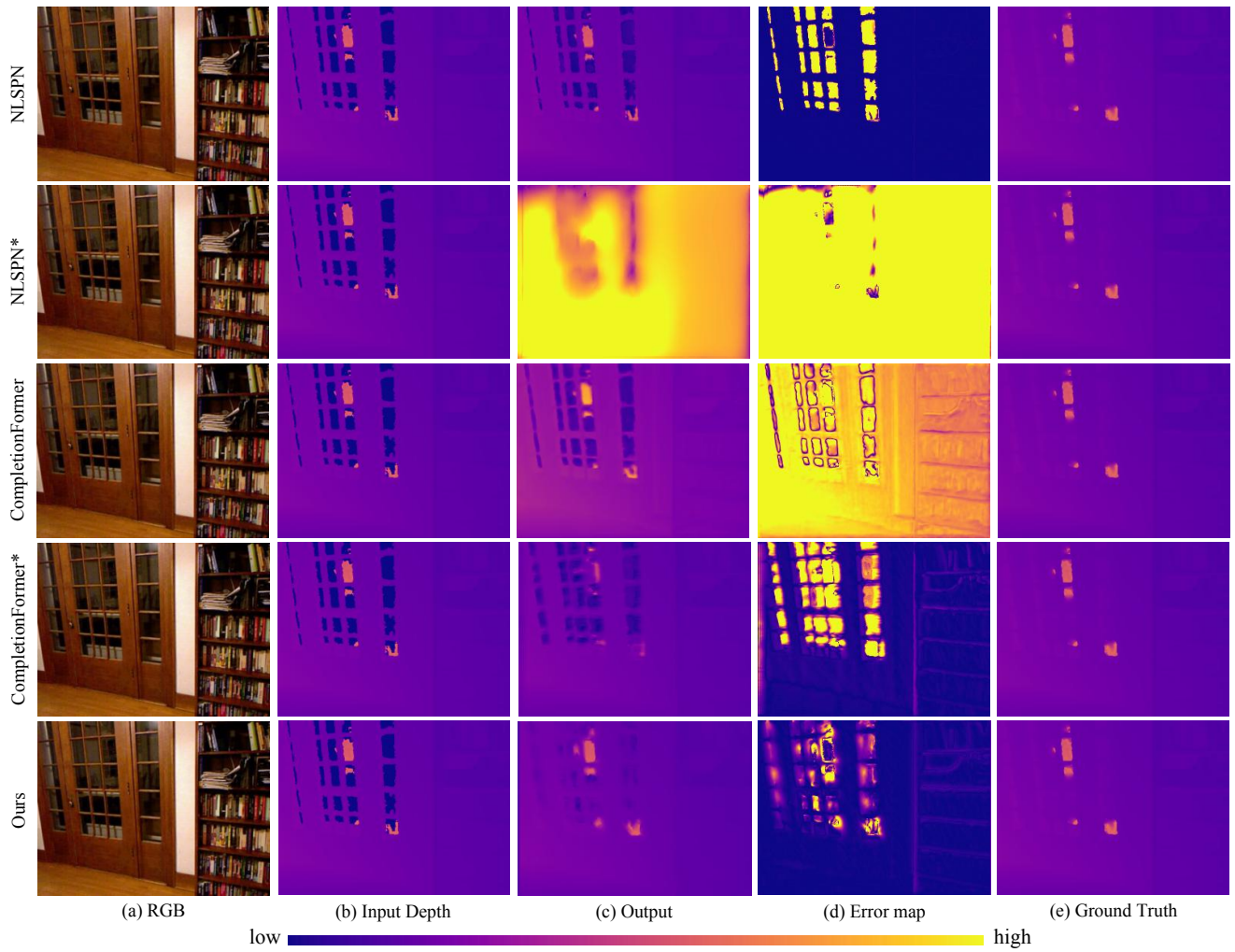


Figure 14. **Qualitative results on SUNRGBD.** * denotes trained model using our training strategy, without * is their released pretrained model trained using fixed patterns.